

Measurement-induced nuclear spin polarization

Zhu-yao Jin,¹ Jia-shun Yan,¹ and Jun Jing^{1,*}

¹*School of Physics, Zhejiang University, Hangzhou 310027, Zhejiang, China*

(Dated: August 22, 2022)

We propose a nuclear-spin polarization protocol in a general evolution-and-measurement framework. The technique works in a spin-star configuration, where the central spin is coupled to the surrounding bath (nuclear) spins by flip-flop interaction and subject to a sequence of projective measurements on its ground state. Then a nondeterministic nuclear-spin polarization could be implemented by entropy reduction through measurement. Optimized measurement-interval τ_{opt} is analytically obtained in the near-resonant condition, which is particularly relevant to the nuclear spins' polarization degree of the last-round measurement, the number of nuclear spins, and the coupling strength between central spin and nuclear spins. Hundreds and even thousands of randomly aligned nuclear spins under thermal state could be almost fully polarized with an optimized sequence of less than twenty unequal-time-spacing measurements. In comparison to the conventional methods, our protocol is not sensitive to the ambient conditions and it is robust against the extra counter-rotating interaction in the near-resonant case.

I. INTRODUCTION

In scalable solid-state devices for quantum information processing, dynamic nuclei polarization (DNP) is of enormous practical importance for spin-based quantum technology and of fundamental interest to state initialization of nuclear spins [1–3]. For various applications, such as nuclear magnetic resonance, magnetic resonance imaging [4–6], discrete-variable quantum computation [7–9], and quantum registers [10], it is desirable to drive the nuclear spins from an initial thermal state to a fully polarized state.

Various routes toward DNP have been actively pursued for a long time, including the continuous [11] and pulsed [12, 13] microwave radiations, the level anti-crossing of the ground [14, 15] or the excited states [16–18], and the field sweeps [19]. Conventional DNP methods have been developed in several highly studied solid-state platforms. By virtue of significant hyperfine interactions, the electron polarization could be transmitted to the nuclear spins [15, 20–22]. In nitrogen-vacancy (NV) center systems, the electronic polarization is pumped to the bulk ^{13}C nuclear spins in diamond [14, 16, 18, 23–27] by optically driving. In quantum dots (QD), DNP has been performed in both single-dot [28] and double-dot [29, 30] systems. A near-perfect polarization (A degree of nearly 90% could be demonstrated in a double quantum-dot system [30]) demands a precise control over the external magnetic field in a narrow regime.

Under a finite-temperature environment, the external magnetic field breaks the polarization symmetry of the nuclear spins in spatial direction and then transforms the target of DNP to a complete purification of the spins. Inspired by the idea of state-purification through repeated projective measurements [31], we here consider the theoretical problem of DNP in a framework of free-evolution-

and-measurement. In particular, when the ground state of the central spin (electron spin) is closely associated with that of the target spins (nuclear spins), a projective measurement on the ground state of the central spin could force the nuclear spins into their ground state. The strategy is nondeterministic with a finite success probability of entropy reduction and has been applied to the ground-state cooling in various scenarios [32–35]. For a two-spin system under the resonant condition, the protocol can be straightforwardly understood by the reduced dynamics of the target spin. Suppose the central spin d is prepared in its ground state and the target spin s in a state described by a Bloch vector (r_x, r_y, r_z) . r_z measures the occupation probability of target spin in the ground state. The interaction Hamiltonian reads $H = g(\sigma_s^+ \sigma_d^- + \sigma_s^- \sigma_d^+)$, where g is the coupling strength. After a joint evolution with a short time τ and measuring the ground state of the central spin, one can find that $r_z \rightarrow r'_z = 1 - \cos^2(g\tau)(1 - r_z) \geq r_z$. Then after certain rounds of evolution-and-measurement with a proper time-spacing, an arbitrary (r_x, r_y, r_z) will approach $(0, 0, 1)$, i.e., the target spin is fully polarized or very close to it.

In this work, we illustrate how this protocol works with a spin-star model by acting the projective measurements on the central (electron) spin. In an ideal situation, the central spin is assumed to couple to the surrounding bath spins with a homogeneous Heisenberg XY interaction. Central spin and bath spins are prepared at the ground state $|g\rangle$ and the thermal state, respectively. For a number of bath spins, DNP could be realized through less than a dozen of rounds of unequal-time-spacing measurements. We derive the analytical expression of the optimized time-spacing for neighboring measurements. Also our protocol is out of the constraint of strong magnetic fields in a narrow regime.

The rest part of this work is structured as follows. In Sec. II, we introduce the spin-star model for polarizing a spin bath by repeated measurements. The protocol is generally described by the polarization coefficients, i.e.,

* Email address: jingjun@zju.edu.cn

the occupation ratios for the nuclear spins in high-excited states. In Sec. III, we derive an analytical expression for iteratively optimizing measurement-interval in the near-resonant condition and constructing an unequal-time-spacing strategy. In Sec. IV, our protocols under both the equal-time-spacing and the unequal-time-spacing strategies are performed for various sizes of spin bath. Then the optimized unequal-time-spacing strategy is applied to feasible systems, including NV centers and QDs. In Sec. V, we discuss the effects from counter-rotating interaction and longitudinal interaction on DNP. We summarize the whole work in Sec. VI.

II. MODEL AND HAMILTONIAN

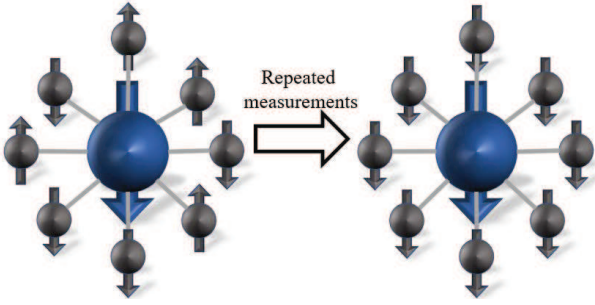


FIG. 1. Diagram of the spin-star model for our polarization-by-measurement protocol. The central (electron) spin (the blue sphere) is homogeneously coupled to the surrounding bath (nuclear) spins (the black spheres), while neglecting the interactions among bath spins. Initially the central spin is at the ground state and the bath spins are at the thermal-equilibrium state. After repeated measurements acting on the central spin, the bath spins could approach a fully polarized state.

Our polarization protocol is based on a spin-star model shown in Fig. 1, consisting of a central spin-1/2 coupled to M surrounding bath spins-1/2 via a homogeneous Heisenberg XY interaction [36]. The full Hamiltonian reads ($\hbar \equiv 1$)

$$H = \frac{\omega_0}{2}\sigma_d^z + \frac{\omega_1}{2}\sum_{j=1}^M\sigma_j^z + g\sum_{j=1}^M(\sigma_d^x\sigma_j^x + \sigma_d^y\sigma_j^y), \quad (1)$$

where ω_0 and ω_1 are the frequencies of the central and bath spins, respectively, g is the homogeneous coupling strength between them, and $\sigma^{x,y,z}$ are Pauli operators. In the rotating frame with respect to $H'_0 = \omega_1/2(\sigma_d^z + \sum_{j=1}^M\sigma_j^z)$, the Hamiltonian can be written as

$$\begin{aligned} H' &= e^{iH'_0 t} H e^{-iH'_0 t} - H'_0 \\ &= \frac{\Delta}{2}\sigma_d^z + 2g\sum_{j=1}^M(\sigma_d^+\sigma_j^- + \sigma_d^-\sigma_j^+), \end{aligned} \quad (2)$$

where $\Delta = \omega_0 - \omega_1$ is the detuning between the central spin and the bath spins and $\sigma^+ = |e\rangle\langle g|$ and $\sigma^- = |g\rangle\langle e|$

are the transition operators. Using the collective angular momentum operators $J_{\pm} \equiv \sum_{j=1}^M\sigma_j^{\pm}$ [37, 38], we have

$$H' = \frac{\Delta}{2}\sigma_d^z + 2g(J_+\sigma_d^- + J_-\sigma_d^+). \quad (3)$$

In this representation, the eigenstates of the spin bath can be denoted by the eigenbasis $\{|m\rangle\}$ of $J_z \equiv \sum_{j=1}^M\sigma_j^z/2$, where m runs from 0 to M [37, 38]. $|m=0\rangle$ implies that M bath spins are all in the ground state and $|m=M\rangle$ implies that they are all in the excited state. Both of them are fully polarized. The collective angular momentum operators [38] satisfy

$$\begin{aligned} J_z|m\rangle &= \left(m - \frac{M}{2}\right)|m\rangle, \\ J_+|m\rangle &= \sqrt{(M-m)(m+1)}|m+1\rangle, \\ J_-|m\rangle &= \sqrt{(M-m+1)m}|m-1\rangle. \end{aligned} \quad (4)$$

The central spin and the bath spins are supposed to be initially separable and respectively at the ground state and the thermal state with a finite temperature T , i.e., $\rho(0) = |g\rangle\langle g| \otimes \rho_s(0)$. Using Eq. (4), the initial state of the bath spins could be written as

$$\rho_s(0) = \sum_{m=0}^M p_m |m\rangle\langle m|, \quad p_m = \frac{1}{Z} e^{-\beta\omega_1(m-M/2)}, \quad (5)$$

where $Z \equiv \text{Tr}[\exp(-\beta\omega_1 J_z)]$ is the partition function and $\beta = 1/(k_B T)$ is the inverse temperature of the spin bath with k_B the Boltzmann constant.

In the framework of free-evolution-and-measurement, our DNP protocol is performed through rounds of joint free-evolution $U(\tau) = \exp(-iH'\tau)$ under the interaction Hamiltonian in Eq. (3) with a time-spacing τ and instantaneous projective measurement $\mathcal{M} \equiv |g\rangle\langle g|$ acting on the ground state of the central spin. Note $|g\rangle|m=0\rangle$ is the global ground state of H' and all the excited states are distributed in the degenerate subspaces ordered by the excitation numbers. The repeated projections over $|g\rangle$ of the central spin therefore dramatically change the dynamics of the bath spins, by discarding their distributions in the manifolds with $|m \neq 0\rangle$. If the measurement outcome turns out that the central spin is not in $|g\rangle$, then the system sample is abandoned and the protocol restarts from the beginning. This strategy is equivalent to reduce the entropy of the whole system conditionally by quantum measurement. Under the equal-time-spacing strategy with N rounds of evolution-and-measurement, the bath state turns out to be

$$\rho_s(N\tau) = \frac{V(\tau)^N \rho_s(0) V^\dagger(\tau)^N}{P(N)}, \quad (6)$$

where $V(\tau) = \langle g|U(\tau)|g\rangle$ constitutes a nonunitary time-evolution operator for the bath spins and $P(N) = \text{Tr}[V(\tau)^N \rho_s(0) V^\dagger(\tau)^N]$ is the success probability of finding the central spin in its ground state $|g\rangle$ at time $t = N\tau$.

In terms of the eigenbasis $\{|m\rangle\}$, we have

$$V(\tau) = \sum_{m=0}^M \alpha_m(\tau) |m\rangle \langle m|, \quad (7)$$

where $\alpha_m(\tau)$ is the polarization coefficient describing the population-reduction ratio on the state $|m\rangle$,

$$\alpha_m(\tau) = \cos(\Omega_m \tau) + i \frac{\Delta \sin(\Omega_m \tau)}{2\Omega_m}, \quad (8)$$

$$\Omega_m \equiv \sqrt{\Delta^2/4 + 4g^2m(M-m+1)}.$$

Using Eqs. (5), (6), and (7), we have

$$\rho_s(N\tau) = \frac{\sum_{m=0}^M |\alpha_m(\tau)|^{2N} p_m |m\rangle \langle m|}{P(N)}, \quad (9)$$

$$P(N) = \sum_{m=0}^M |\alpha_m(\tau)|^{2N} p_m.$$

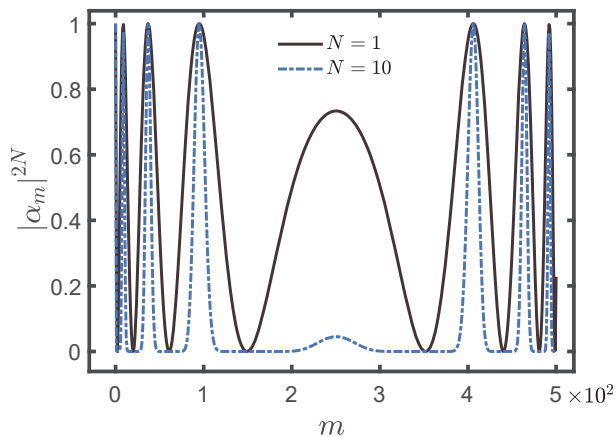


FIG. 2. Polarization coefficient $|\alpha_m(\tau)|^{2N}$ as a function of the eigenbasis index (the magnetic quantum number) m for J_z by a single measurement (the black solid lines) and 10 equal-time-spacing measurements (the blue dot-dashed lines) on the ground state of the central spin coupled to $M = 500$ bath spins. The detuning between the central spin and the bath spins is $\Delta/\omega_0 = 0.1$, the coupling strength is $g/\omega_0 = 0.8$, and the measurement interval is $\omega_0\tau = 0.03$.

Our polarization-by-measurement protocol is self content by the fact that $|\alpha_m(\tau)|^2 \leq 1$, where the equivalence is achieved when $m = 0$ or $\Omega_m\tau = k\pi$. The populations over the other states are gradually reduced by $p_m \rightarrow |\alpha_m(\tau)|^{2N} p_m$. The reduction rate is clearly determined by τ due to Eq. (8). Although the probability of the bath spins in the fully polarized state $|m = 0\rangle$ could be significantly increased by repeated measurements, the polarization coefficients shown in Fig. 2 indicate that under the strategy of equal-time-spacing measurements, there would be always several excited states under protection. A thermal state with a finite temperature will thus be reduced to a classical mixture of a fully polarized

state $|m = 0\rangle$ and those states satisfying $\Omega_m\tau = k\pi$. We are then motivated to find an optimized measurement-interval τ_{opt} and employ an unequal-time-spacing strategy to improve the performance of our polarization protocol.

III. OPTIMIZED MEASUREMENT-INTERVAL AND UNEQUAL-TIME-SPACING STRATEGY

To see more clearly the effect of the measurement interval τ on DNP, we first define a polarization degree of bath spins as

$$\mathcal{P}(t) = \left| \frac{\text{Tr}[J_z \rho_s(t)]}{M/2} \right| = \frac{\sum_{m=0}^M p_m(t)(M/2 - m)}{M/2}, \quad (10)$$

where $p_m(t)$ is the current population over $|m\rangle$. $\mathcal{P}(t)$ ranges from 0 (the most mixed state) to 1 (the fully polarized state) and is consistent with the previous definitions [39, 40], i.e., $\mathcal{P} = (M_\uparrow - M_\downarrow)/M$, where M_\uparrow (M_\downarrow) is the number of the nuclear spins in the up (down) states. Using Eq. (9), we have

$$\mathcal{P}(N) \equiv \mathcal{P}(t = N\tau) = \frac{\sum_{m=0}^M (M/2 - m) |\alpha_m|^{2N} p_m}{M/2 \sum_{m=0}^M |\alpha_m|^{2N} p_m}. \quad (11)$$

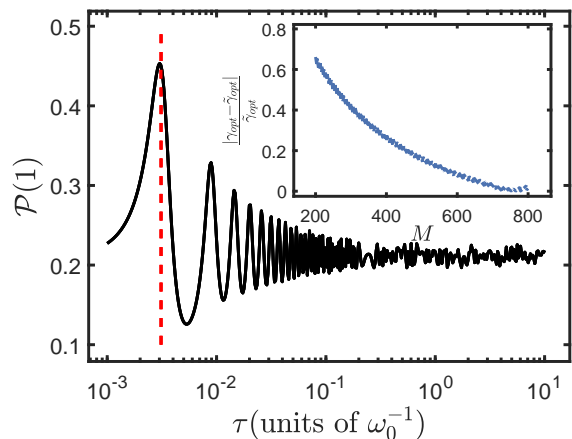


FIG. 3. Polarization degree of $M = 700$ bath spins after one measurement as a function of the measurement-interval τ . The black solid curve is numerically obtained by Eq. (11). The vertical red dashed line is the analytical result for the optimized interval τ_{opt} in Eq. (14). Inset: Relative error of the analytical result for the optimized interval τ_{opt} in comparison to the numerical result $\tilde{\tau}_{\text{opt}}$ as a function of the bath-spin number M . The other parameters are set as $\Delta/\omega_0 = 0.1$, $g/\omega_0 = 0.8$, and $T = 0.5$ K.

A typical observation about the quantitative effect of τ on \mathcal{P} presents in Fig. 3 with $N = 1$ and $M = 700$. The polarization degree is not a monotonic function of τ . It increases rapidly with increasing τ to the maximum value

until an optimized measurement-interval τ_{opt} , and then decreases rapidly to a lower value than that determined by the initial temperature. Afterwards, it fluctuates with a decreasing magnitude and asymptotically approaches the initial polarization. An inappropriate choice of the measurement-interval τ yields thus either inefficient polarization or even depolarization. To locate the optimized τ in proximity to a dramatic-change point of the curve for the highest $\mathcal{P}(1)$, it is interesting to find a local minimum of the denominator in Eq. (11) with $N = 1$, which is a summation over $|\alpha_m|^2$ with the weight p_m . The occupation probability p_m given by Eq. (5) declines monotonically with increasing m , and around $m = 0$ and $\tau = 0$, the polarization coefficient can be approximated by

$$\begin{aligned} |\alpha_m(\tau)|^2 &= 1 - \Omega_m'^2 \frac{\sin^2(\Omega_m \tau)}{\Omega_m^2} \\ &= 1 - \Omega_m'^2 \tau^2 + \left(\Omega_m'^2 + \frac{\Delta^2}{4} \right) \Omega_m'^2 \frac{\tau^4}{3} + \mathcal{O}(\tau^6) \end{aligned} \quad (12)$$

with $\Omega_m' \equiv 2g\sqrt{m(M-m+1)} = \sqrt{\Omega_m^2 - \Delta^2/4}$. Thus the polarization degree is rewritten as

$$\begin{aligned} \mathcal{P}(1) &= \frac{\sum_{m=0}^M (M/2 - m)x^m |\alpha_m|^2}{M/2 \sum_{m=0}^M x^m |\alpha_m|^2} \\ &\approx \frac{\sum_{m=0}^M (M/2 - m)x^m |\alpha_m|^2}{M/2 \sum_{m=0}^M x^m (1 - \Omega_m'^2 \tau^2)} \\ &\approx \frac{\sum_{m=0}^M (M/2 - m)x^m |\alpha_m|^2 / (M/2)}{\sum_{m=0}^{\infty} x^m (1 - \Omega_m'^2 \tau^2)} \\ &= \frac{\sum_{m=0}^M (M/2 - m)x^m |\alpha_m|^2 / (M/2)}{\sum_{m=0}^{\infty} x^m + 4g^2 \tau^2 \sum_{m=0}^{\infty} [m^2 - (M+1)m]x^m} \end{aligned} \quad (13)$$

with $x \equiv \exp(-\beta\omega_1)$. An approximate ‘‘singularity’’ in Eq. (13) emerges as

$$\begin{aligned} \tau_{\text{opt}} &= \sqrt{\frac{\sum_{m=0}^{\infty} x^m}{4g^2 \sum_{m=0}^{\infty} [(M+1)mx^m - m^2x^m]}} \\ &= \sqrt{\frac{1}{4g^2[(M+1)x/(1-x) - (1+x)x/(1-x)^2]}} \\ &= \frac{1}{gM\sqrt{2(1-\mathcal{P}_{\text{th}})\mathcal{P}_{\text{th}}}}, \end{aligned} \quad (14)$$

where we have used the geometric series

$$\sum_{m=0}^{\infty} m^2 x^m = \frac{(1+x)x}{(1-x)^3}, \quad \sum_{m=0}^{\infty} mx^m = \frac{x}{(1-x)^2}, \quad (15)$$

and \mathcal{P}_{th} is the initial polarization degree,

$$\begin{aligned} \mathcal{P}_{\text{th}} &= \frac{\sum_{m=0}^M (M/2 - m)p_m}{M/2 \sum_{m=0}^M p_m} \approx \frac{\sum_{m=0}^{\infty} (M/2 - m)x^m}{M/2 \sum_{m=0}^{\infty} x^m} \\ &= 1 - \frac{2x}{M(1-x)}. \end{aligned} \quad (16)$$

Remark that the upper-bound M for some of the summations in Eqs. (13), (14), and (16) has been approximated by infinity to attain a compact analytical expression. Such that the singularity from a vanishing denominator in $\mathcal{P}(1)$ does not really exist and τ_{opt} is then an estimation used to locate a maximum $\mathcal{P}(1)$. The second-order perturbative optimized measurement-interval τ_{opt} is irrelevant to the detuning Δ between the central spin and the bath spins due to Eq. (12), so that Eq. (14) applies to both resonant and near-resonant situations. τ_{opt} is marked with the vertical red dashed line in Fig. 3, which matches perfectly with the point for obtaining a peak value for \mathcal{P} . The inset in Fig. 3 describes the relative error between the analytical and numerical results for the optimized interval, $|\tau_{\text{opt}} - \tilde{\tau}_{\text{opt}}|/\tilde{\tau}_{\text{opt}}$, as a function of the bath-spin number M . The error magnitude decreases monotonically with increasing M . When $M \geq 560$, it becomes less than 10%. When $M = 700$, it is about 2.5%, consistent with the result in the main plot in Fig. 3.

The population distributions p_m over the eigenstates $\{|m\rangle\}$ and the polarization degree of the spin-bath would be modified after the first round of evolution-and-measurement during an interval τ_{opt} determined by \mathcal{P}_{th} in Eq. (16). An unequal-time-spacing strategy therefore emerges by iteratively updating \mathcal{P}_{th} with the polarization degree of the last round. The optimized measurement-interval expression in Eq. (14) could be reinterpreted as

$$\tau_{\text{opt}}(t) = \frac{1}{gM\sqrt{2[1-\mathcal{P}(t)]\mathcal{P}(t)}}, \quad (17)$$

where $\mathcal{P}(t)$ represents the current polarization degree of bath spins. In practice, given $\tau_{\text{opt}}(t)$ of the last round, the density matrix of spin bath can be obtained by Eq. (9) and then the current polarization degree is calculated by Eq. (10) without measurement. Rather than an equal-time-spacing sequence, Eq. (17) gives rise to an unequal-time-spacing one: $\{\tau_{\text{opt}}(t_1), \tau_{\text{opt}}(t_2), \dots, \tau_{\text{opt}}(t_N)\}$ with $t_{i>1} = \sum_{j=1}^{i-1} \tau_{\text{opt}}(t_j)$ and $\tau_{\text{opt}}(t_1) = \tau_{\text{opt}}$. When $\mathcal{P}(t)$ approaches unit during the DNP process, $\tau_{\text{opt}}(t)$ becomes even larger, meaning that a further polarization becomes more difficult.

Under the unequal-time-spacing protocol, the state of the spin-bath in Eq. (9) is transformed to

$$\rho_s \left[\sum_{i=1}^N \tau_{\text{opt}}(t_i) \right] = \frac{\sum_{m=0}^M \prod_{i=1}^N |\alpha_m[\tau_{\text{opt}}(t_i)]|^2 p_m |m\rangle\langle m|}{P(N)} \quad (18)$$

after N measurements, and the success probability becomes

$$P(N) = \sum_{m=0}^M \prod_{i=1}^N |\alpha_m[\tau_{\text{opt}}(t_i)]|^2 p_m. \quad (19)$$

Now one can find that the variable for the polarization coefficient α_m becomes time-dependent and then all the excited state are no longer under protection when $N > 1$.

IV. POLARIZATION PERFORMANCE

A. Polarization performance under near-resonant condition

In this subsection, we demonstrate the polarization performance of the bath-spins in the NV center system [41] with the equal-time-spacing or unequal-time-spacing polarization-by-measurement strategies under the near-resonant condition. Accordingly, the optimized measurement-interval τ_{opt} is then found by Eqs. (14) or (17). In numerical evaluations, the eigenfrequency of the central (electron) spin is chosen as $\omega_0 = 120$ MHz. The detuning between central spin and bath spins and their coupling strength are fixed as $\Delta/\omega_0 = 0.1$ and $g/\omega_0 = 0.03$, respectively. And the spin bath is initialized with a temperature $T = 0.5$ K.

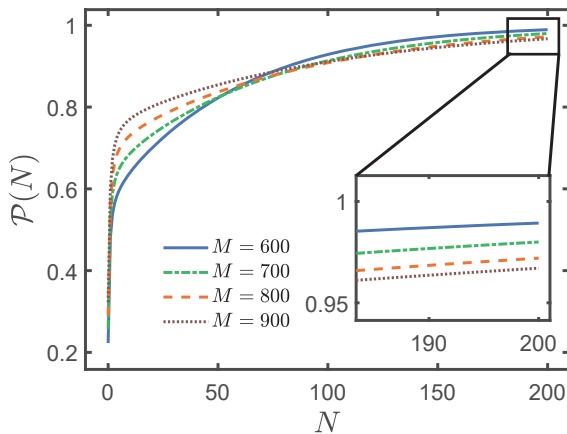


FIG. 4. Polarization degree of nuclear spins $\mathcal{P}(N)$ as a function of the measurement number N under the equal-time-spacing strategy with various size of the nuclear spin-bath. The blue solid line, the green dot-dashed line, the orange dashed line, and the brown dotted line represent $M = 600, 700, 800$ and 900 , respectively. The other parameters are set as $\Delta/\omega_0 = 0.1$, $g/\omega_0 = 0.03$, and $T = 0.5$ K.

Figure 4 demonstrates the performance of the equal-time-spacing strategy on the spin bath with various size. According to Eqs. (14) and (16), a larger size of spin-bath yields a smaller τ_{opt} and a higher initial polarization degree \mathcal{P}_{th} . In particular, for $M = 600$, $\mathcal{P}_{\text{th}} = 0.223$; for $M = 700$, $\mathcal{P}_{\text{th}} = 0.257$; for $M = 800$, $\mathcal{P}_{\text{th}} = 0.290$; and for $M = 900$, $\mathcal{P}_{\text{th}} = 0.322$. In the first dozens of rounds of measurements, the polarization rate of a larger size of spin-bath is higher than that of a smaller size. And the former becomes lower than the latter as more measurements are carried out. At around $N = 75$, the four curves cross with each other. With even more measurements, a smaller M yields a slightly bigger asymptotic value of $\mathcal{P}(N)$. When $N = 200$, it is found in the inset of Fig. 4 that for $M = 600$, $\mathcal{P} = 0.989$; for $M = 700$, $\mathcal{P} = 0.980$; for $M = 800$, $\mathcal{P} = 0.972$; and for $M = 900$, $\mathcal{P} = 0.967$. On the whole, the polarization

degrees $\mathcal{P}(N)$ could be enhanced from their initial values to nearly unit by a sufficiently large number of rounds of evolution-and-measurement. The decreasing polarization rates under the equal-time-spacing strategy indicate explicitly that the optimized measurement-interval determined by the initial thermal-state polarization degree \mathcal{P}_{th} becomes even more inefficient for the subsequent rounds of measurement, as can be predicted by Eq. (14).

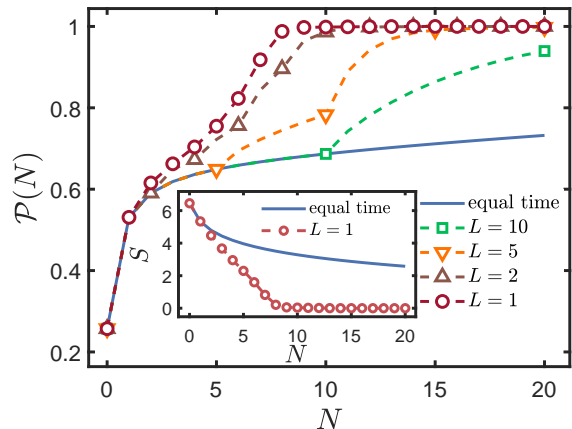


FIG. 5. Polarization degree of $M = 700$ nuclear spins as a function of measurement number N under various polarization strategies. The blue solid line represents the equal-time-spacing strategy. The green dashed line with square markers, the orange dashed line with inverted-triangle markers, the brown dashed line with triangle markers, and the red dashed line with circle markers represent the unequal-time-spacing strategies in which the measurement interval is updated every $L = 10, 5, 2, 1$ rounds of evolution-and-measurement, respectively. Inset: The Von Neumann entropy S of spin-bath as a function of measurement number N . The other parameters are the same as Fig. 4.

The equal-time-spacing strategy is only optimized in the first round of the sequence. To enhance the polarization performance by accurately locate every peak value of the polarization degree under one measurement, one has to iterate the optimized measurement-interval according to Eq. (17). In Fig. 5, we present the dynamics of the polarization degree for $M = 700$ nuclear spins under the equal-time-spacing strategy and four unequal-time-spacing strategies with various iterative rate L . For example, $L = 5$ means that the measurement-interval $\tau_{\text{opt}}(t)$ is updated every five rounds of evolution-and-measurement. Accordingly, equal-time-spacing strategy means $L \rightarrow \infty$. And for $L = 1$, we have $\tau_{\text{opt}}(t_i) < \tau_{\text{opt}}(t_{i+1})$ in the true sense of unequal-time-spacing strategy. It is observed that more-frequent updating of the optimized measurement-interval gives rise to better polarization performance. In particular, one has to run the strategy with $L = 5$ for $N = 15$ rounds or run that with $L = 1$ for only $N = 8$ rounds to achieve $\mathcal{P} > 0.99$. In comparison to the equal-time-spacing strategy in Fig. 4, the number of measurements is reduced by one order un-

der the unequal-time-spacing strategy, demonstrating a dramatic advantage in experimental overhead.

The polarization effect by measurements could be understood by the dynamics of the Von Neumann entropy of the bath spins. It is evaluated by

$$S[\rho_s(t)] = - \sum_{m=0}^M p_m(t) \ln p_m(t), \quad (20)$$

where ρ_s is given by Eq. (9) for the equal-time-spacing strategy and by Eq. (18) for the unequal-time-spacing strategy, respectively. We provide these two results in the inset of Fig. 5. Clearly the enhancement of the polarization degree is accompanied with the entropy reduction. Also S could be used to demonstrate the power of the unequal-time-spacing strategy. In particular, for the equal-time-spacing strategy, when $N = 9$, $S = 3.39$ and when $N = 20$, $S = 2.58$; for $L = 1$, when $N = 9$, $S = 0.05$ and when $N = 20$, $S \approx 10^{-5}$.

B. Polarization performance under far off-resonant condition

In this subsection, the application of the unequal-time-spacing strategy is extended to the far off-resonant condition. According to Eq. (12), the analytical expression for either τ_{opt} in Eq. (14) or $\tau_{\text{opt}}(t)$ in Eq. (17) becomes invalid in the presence of a significant Δ/ω_0 . In this case, especially for a typical QD system (see Tab. I), $\tau_{\text{opt}}(t)$ can be obtained by numerical simulation.

| | M ($\times 10^2$) | B (G) | ω_0 (MHz) | Δ/ω_0 | g/ω_0 |
|-------------------|---------------------|-------|------------------|-------------------|--------------|
| NV ⁽¹⁾ | 5 | 1000 | 120 | 0.1 | 0.03 |
| NV ⁽²⁾ | 5 | 900 | 400 | 0.95 | 0.03 |
| | M ($\times 10^3$) | B (G) | ω_0 (GHz) | Δ/ω_0 | g/ω_0 |
| QD ⁽¹⁾ | 2 | 379 | 5 | 0.999 | 0.016 |
| QD ⁽²⁾ | 2 | 758 | 10 | 0.999 | 0.008 |

TABLE I. Experimental parameters, including bath size, magnetic field strength, frequencies of central spin and bath spin, and detuning, for various NV center systems [41] and QD systems [42, 43]. For the latter, the gyromagnetic ratio of the electron spin is three orders of magnitude greater than that of the surrounding nuclear spins, that generally gives rise to a far off-resonant condition.

In Fig. 6, we present the performance of the unequal-time-spacing strategy on the four cases listed in Tab. I. For the NV-center systems, we consider both a near-resonant case [see the blue dashed line with circle markers for NV⁽¹⁾] and a far-off-resonant case [see the green dashed line with square markers for NV⁽²⁾]. The initial thermal-state polarization degree for NV⁽¹⁾ is significantly larger than that for NV⁽²⁾. So that the off-resonant case requires more measurements to achieve the same polarization degree of the resonant case. In particular, for NV⁽¹⁾, $\mathcal{P}(8) = 0.997$ and for NV⁽²⁾, $\mathcal{P}(8) = 0.968$.

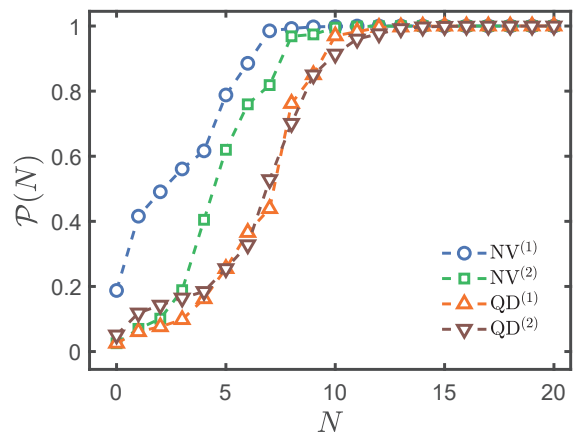


FIG. 6. Polarization degree of bath spins as a function of measurement number N for NV center systems (the blue dashed line with circle markers and the green dashed line with square markers) and QD systems (the orange dashed line with triangle markers and the brown dashed line with inverted-triangle markers) listed in Tab. I. $T = 0.5$ K and the other parameters are set as Tab. I.

While both of them saturate to nearly unit when $N = 12$. With more nuclear spins in the bath and the three-order distance in the magnitude of the gyromagnetic ratios for the central and the bath spins, the polarization degrees in QD systems (see the orange dashed line with triangle markers and the brown dashed line with inverted-triangle markers in Fig. 6) are significantly lower than those in NV-center systems in the first several rounds. But when $N \geq 10$, they can be enhanced to over 0.90. In particular, for QD⁽¹⁾, $\mathcal{P}(10) = 0.970$ and for QD⁽²⁾, $\mathcal{P}(10) = 0.914$. And they can be almost completely polarized by $N = 15$ measurements.

In the NV-center systems, a nearly complete polarization of nuclear spins has been realized by constructing a near-resonant condition around the ground state level anti-crossing [15, 41], which demands a precise control over the external magnetic field ($B \sim 0.1$ T). In the QD systems [30], a less than 90% degrees of polarization could be realized under a low temperature and a strong external magnetic field for nuclear spins. In comparison to these conventional methods, our protocol of the unequal-time-spacing strategy could achieve a complete polarization of nuclear spins with less than a dozen of rounds of evolution-and-measurement, regardless of a precisely-controlled external conditions, for both NV-center and QD systems.

V. DISCUSSION

In our spin-star model, the preceding polarization-by-measurement protocols are based on the Heisenberg XY interaction between central spin and bath spins, by which they can faithfully exchange their polarized states. In

this section, we discuss the effects from two extra interactions on the polarization performance, which might present in practical interactions. The results are obtained under the unequal-time-spacing strategy with the iteratively optimized measurement-intervals in Eq. (17).

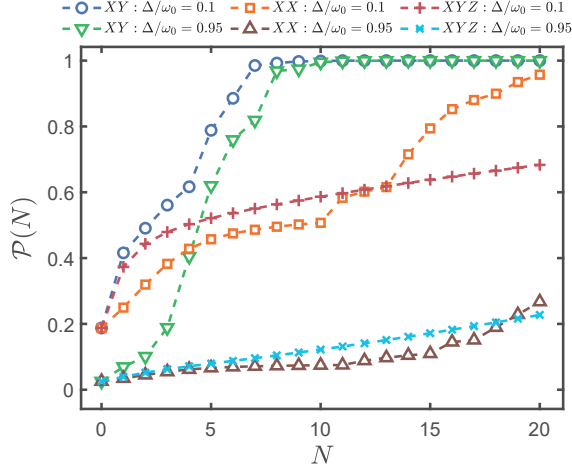


FIG. 7. Polarization degree of $M = 500$ bath spins as a function of the measurement number N in the presence of various interaction and detuning between central spin and bath spins. For XY interaction, the blue dashed line with circle markers and the green dashed line with inverted-triangle markers represent the near-resonant ($\Delta/\omega_0 = 0.1$) and far-off-resonant cases ($\Delta/\omega_0 = 0.95$), respectively. For XX interaction, the orange dashed line with square markers and the brown dashed line with triangle markers represent the near-resonant ($\Delta/\omega_0 = 0.1$) and far-off-resonant cases ($\Delta/\omega_0 = 0.95$), respectively. For XYZ interaction, the red dashed line with plus markers and the cyan dashed line with cross markers represent the near-resonant ($\Delta/\omega_0 = 0.1$) and far-off-resonant cases ($\Delta/\omega_0 = 0.95$), respectively. The other parameters are set as $g/\omega_0 = 0.03$ and $T = 0.5$ K.

First, we consider the Heisenberg XX interaction between the central spin and the bath spins, which is equivalent to include the time-dependent counter-rotating terms into the flip-flop interaction in the interaction picture. Then using the collective angular momentum operators, the full Hamiltonian in the Schrödinger picture can be written as

$$\begin{aligned} H &= H_0 + H_I, \\ H_0 &= \frac{\omega_0}{2} \sigma_d^z + \omega_1 J_z, \\ H_I &= 2g (\sigma_d^+ J_- + \sigma_d^- J_+) + 2g (\sigma_d^+ J_+ + \sigma_d^- J_-). \end{aligned} \quad (21)$$

The last counter-rotating terms are conventionally neglected when $g \ll \omega_0, \omega_1, |\Delta|$. Second, we can consider the Heisenberg XYZ interaction, i.e., there is a longitudinal interaction in addition to the transverse interaction between the central spin and the bath spins. In the rotating frame with respect to $H'_0 = \omega_1/2(\sigma_d^z + J_z)$, the full Hamiltonian can be written as

$$H' = \frac{\Delta}{2} \sigma_d^z + 2g (J_+ \sigma_d^- + J_- \sigma_d^+) + g J_z \sigma_d^z. \quad (22)$$

In Fig. 7, we demonstrate the polarization performances under various interaction and detuning Δ/ω_0 within $N = 20$ rounds of measurements. With a fixed number of bath spins, a smaller detuning gives rise to a larger thermal-state polarization \mathcal{P}_{th} and also a better polarization performance for any interaction between central spin and bath spins. The presence of either counter-rotating interaction or longitudinal interaction always suppress the polarization effect by our measurement protocol, which becomes significant in the far-off-resonant situation. In particular, when $\Delta/\omega_0 = 0.1$, it is found for XY interaction, $\mathcal{P}(8) = 0.99$; for XX interaction, $\mathcal{P}(20) = 0.96$; and for XYZ interaction, $\mathcal{P}(20) = 0.68$. When $\Delta/\omega_0 = 0.95$, for XY interaction, $\mathcal{P}(10) = 0.99$; for XX interaction, $\mathcal{P}(20) = 0.27$; and for XYZ interaction, $\mathcal{P}(20) = 0.23$. The presence of the counter-rotating interaction, especially under a far-off-resonant condition, can not be ignored, although we are working in a weak-coupling regime $g/\omega_0 = 0.03$. When $N \leq 13$, the polarization degree of the bath spins under XYZ interaction is higher than that under XX interaction, yet roughly it is found the suppression effect from the longitudinal interaction is more severe than that from the counter-rotating interaction.

VI. CONCLUSION

In summary, we propose a measurement-based dynamical nuclear-spin polarization protocol in a spin-star model, where the central spin is homogeneously coupled to the surrounding bath spins with the Heisenberg XY interaction. The central spin and the bath spins are prepared at the ground state and the thermal equilibrium state, respectively. We show that the bath spins could be nearly completely polarized through repeated instantaneous projective measurement performed on the ground state of the central spin. The polarization performance can be significantly promoted by optimizing the measurement interval τ_{opt} , which is determined by the polarization degree at the end of last round of evolution-and-measurement, the size of the spin bath, and the coupling strength between central spin and bath spins. Our protocol favors the unequal-time-spacing strategy in which the optimized measurement-interval is updated every round and the near-resonant condition between central spin and bath spins. With an ideal unequal-time-spacing strategy, the polarization degree of nuclear spins could be completely polarized in less than a dozen of measurements, for both NV center and QD systems. They are scalable solid-state systems and good candidates for various quantum technology applications.

Our polarization-by-measurement protocol can be considered as an extension of measurement-based cooling that originates from cooling mechanical oscillators in optomechanics, in which repeated measurements on the ground state of the ancillary system generate fast cooling with a finite success probability. Our method is different

from the quantum Zeno effect (QZE) for which it was predicted and verified that frequent, controlled measurements into a fixed state or subspace can inhibit a quantum system from leaving that state or subspace. Rather than taking the measurement interval to zero in the limit for QZE, we find that the probability in which a scalable and randomly aligned spin system stays at the polarized state or subspace can be steadily accumulated through

measurements with optimized intervals.

ACKNOWLEDGMENTS

We acknowledge financial support from the National Science Foundation of China (Grants No. 11974311 and No. U1801661).

-
- [1] A. Abragam, *The principles of nuclear magnetism*, 32 (Oxford university press, 1961).
- [2] F. Meier and B. P. Zakharchenya, *Optical orientation* (Elsevier, 2012).
- [3] P. T. Callaghan, *Principles of nuclear magnetic resonance microscopy* (Oxford University Press on Demand, 1993).
- [4] J. H. Ardenkjær-Larsen, B. Fridlund, A. Gram, G. Hansson, L. Hansson, M. H. Lerche, R. Servin, M. Thaning, and K. Golman, *Increase in signal-to-noise ratio of > 10,000 times in liquid-state nmr*, *Proc. Natl. Acad. Sci.* **100**, 10158 (2003).
- [5] A. G. Rankin, J. Trébosc, F. Pourpoint, J.-P. Amoureux, and O. Lafon, *Recent developments in mas dnp-nmr of materials*, *Solid State Nucl. Magn. Res.* **101**, 116 (2019).
- [6] V. Denysenkov, M. Terekhov, R. Maeder, S. Fischer, S. Zangos, T. Vogl, and T. Prisner, *Continuous-flow dnp polarizer for mri applications at 1.5 t*, *Sci. Rep.* **7**, 1 (2017).
- [7] B. E. Kane, *A silicon-based nuclear spin quantum computer*, *Nature* **393**, 133 (1998).
- [8] H. Schwager, J. I. Cirac, and G. Giedke, *Quantum interface between light and nuclear spins in quantum dots*, *Phys. Rev. B* **81**, 045309 (2010).
- [9] C. Kloeffel and D. Loss, *Prospects for spin-based quantum computing in quantum dots*, *Annu. Rev. Condens. Matter. Phys.* **4**, 51 (2013).
- [10] M. V. G. Dutt, L. Childress, L. Jiang, E. Togan, J. Maze, F. Jelezko, A. S. Zibrov, P. R. Hemmer, and M. D. Lukin, *Quantum register based on individual electronic and nuclear spin qubits in diamond*, *Science* **316**, 1312 (2007).
- [11] A. Abragam and W. G. Proctor, *A new method of dynamic polarization of atomic nuclei in solids*, *Compt. Rend.* **246** (1958).
- [12] A. Henstra, P. Dirksen, J. Schmidt, and W. Wenckebach, *Nuclear spin orientation via electron spin locking (novel)*, *J. Magn. Reson.* **77**, 389 (1988).
- [13] A. Henstra, P. Dirksen, and W. T. Wenckebach, *Enhanced dynamic nuclear polarization by the integrated solid effect*, *Phys. Lett. A* **134**, 134 (1988).
- [14] H.-J. Wang, C. S. Shin, C. E. Avalos, S. J. Seltzer, D. Budker, A. Pines, and V. S. Bajaj, *Sensitive magnetic control of ensemble nuclear spin hyperpolarization in diamond*, *Nat. Commun.* **4**, 1 (2013).
- [15] P. Wang, B. Liu, and W. Yang, *Strongly polarizing weakly coupled ^{13}C nuclear spins with optically pumped nitrogen-vacancy center*, *Sci. Rep.* **5**, 1 (2015).
- [16] R. Fischer, C. O. Bretschneider, P. London, D. Budker, D. Gershoni, and L. Frydman, *Bulk nuclear polarization enhanced at room temperature by optical pumping*, *Phys. Rev. Lett.* **111**, 057601 (2013).
- [17] R. Wunderlich, J. Kohlrantz, B. Abel, J. Haase, and J. Meijer, *Optically induced cross relaxation via nitrogen-related defects for bulk diamond ^{13}C hyperpolarization*, *Phys. Rev. B* **96**, 220407 (2017).
- [18] D. Pagliero, K. R. K. Rao, P. R. Zangara, S. Dhomkar, H. H. Wong, A. Abril, N. Aslam, A. Parker, J. King, C. E. Avalos, A. Ajoy, J. Wrachtrup, A. Pines, and C. A. Meriles, *Multispin-assisted optical pumping of bulk ^{13}C nuclear spin polarization in diamond*, *Phys. Rev. B* **97**, 024422 (2018).
- [19] J. Henshaw, D. Pagliero, P. R. Zangara, M. B. Franzoni, A. Ajoy, R. H. Acosta, J. A. Reimer, A. Pines, and C. A. Meriles, *Carbon-13 dynamic nuclear polarization in diamond via a microwave-free integrated cross effect*, *Proc. Natl. Acad. Sci.* **116**, 18334 (2019).
- [20] C.-W. Huang and X. Hu, *Theoretical study of nuclear spin polarization and depolarization in self-assembled quantum dots*, *Phys. Rev. B* **81**, 205304 (2010).
- [21] V. Jacques, P. Neumann, J. Beck, M. Markham, D. Twitchen, J. Meijer, F. Kaiser, G. Balasubramanian, F. Jelezko, and J. Wrachtrup, *Dynamic polarization of single nuclear spins by optical pumping of nitrogen-vacancy color centers in diamond at room temperature*, *Phys. Rev. Lett.* **102**, 057403 (2009).
- [22] I. Neder, M. S. Rudner, and B. I. Halperin, *Theory of coherent dynamic nuclear polarization in quantum dots*, *Phys. Rev. B* **89**, 085403 (2014).
- [23] G. A. Álvarez, C. O. Bretschneider, R. Fischer, P. London, H. Kanda, S. Onoda, J. Isoya, D. Gershoni, and L. Frydman, *Local and bulk ^{13}C hyperpolarization in nitrogen-vacancy-centred diamonds at variable fields and orientations*, *Nat. Commun.* **6**, 1 (2015).
- [24] A. Ajoy, K. Liu, R. Nazaryan, X. Lv, P. R. Zangara, B. Safvati, G. Wang, D. Arnold, G. Li, A. Lin, P. Raghavan, E. Druga, S. Dhomkar, D. Pagliero, J. A. Reimer, D. Suter, C. A. Meriles, and A. Pines, *Orientation-independent room temperature optical ^{13}C hyperpolarization in powdered diamond*, *Sci. Adv.* **4**, eaar5492 (2018).
- [25] A. Ajoy, R. Nazaryan, K. Liu, X. Lv, B. Safvati, G. Wang, E. Druga, J. A. Reimer, D. Suter, C. Ramanathan, C. A. Meriles, and A. Pines, *Enhanced dynamic nuclear polarization via swept microwave frequency combs*, *Proc. Natl. Acad. Sci.* **115**, 10576 (2018).
- [26] A. Ajoy, R. Nazaryan, E. Druga, K. Liu, A. Aguilar, B. Han, M. Gierth, J. T. Oon, B. Safvati, R. Tsang, et al., *Room temperature “optical nanodiamond hyperpolarizer”: Physics, design, and operation*, *Rev. Sci. Instrum.* **91**, 023106 (2020).
- [27] A. Ajoy, A. Sarkar, E. Druga, P. Zangara, D. Pagliero, C. Meriles, and J. Reimer, *Low-field microwave-mediated optical hyperpolarization in optically pumped diamond*, *J.*

- Magn. Reson. **331**, 107021 (2021).
- [28] C. F. Fong, Y. Ota, S. Iwamoto, and Y. Arakawa, *Manipulation of dynamic nuclear spin polarization in single quantum dots by photonic environment engineering*, *Phys. Rev. B* **95**, 245423 (2017).
- [29] M. Gullans, J. J. Krich, J. M. Taylor, H. Bluhm, B. I. Halperin, C. M. Marcus, M. Stopa, A. Yacoby, and M. D. Lukin, *Dynamic nuclear polarization in double quantum dots*, *Phys. Rev. Lett.* **104**, 226807 (2010).
- [30] M. J. A. Schuetz, E. M. Kessler, L. M. K. Vandersypen, J. I. Cirac, and G. Giedke, *Nuclear spin dynamics in double quantum dots: Multistability, dynamical polarization, criticality, and entanglement*, *Phys. Rev. B* **89**, 195310 (2014).
- [31] H. Nakazato, T. Takazawa, and K. Yuasa, *Purification through zeno-like measurements*, *Phys. Rev. Lett.* **90**, 060401 (2003).
- [32] R. Puebla, O. Abah, and M. Paternostro, *Measurement-based cooling of a nonlinear mechanical resonator*, *Phys. Rev. B* **101**, 245410 (2020).
- [33] P. V. Pyshkin, D.-W. Luo, J. Q. You, and L.-A. Wu, *Ground-state cooling of quantum systems via a one-shot measurement*, *Phys. Rev. A* **93**, 032120 (2016).
- [34] J.-s. Yan and J. Jing, *External-level assisted cooling by measurement*, *Phys. Rev. A* **104**, 063105 (2021).
- [35] J.-s. Yan and J. Jing, *Simultaneous cooling by measuring one ancillary system*, *Phys. Rev. A* **105**, 052607 (2022).
- [36] J. Jing and Z.-G. Lü, *Dynamics of two qubits in a spin bath with anisotropic xy coupling*, *Phys. Rev. B* **75**, 174425 (2007).
- [37] Z. Wang, Y. Guo, and D. Zhou, *Non-markovian dynamics in a spin star system: the failure of thermalisation*, *Eur. Phys. J. D* **67**, 1 (2013).
- [38] Y. Hamdouni, M. Fannes, and F. Petruccione, *Exact dynamics of a two-qubit system in a spin star environment*, *Phys. Rev. B* **73**, 245323 (2006).
- [39] C. Deng and X. Hu, *Analytical solution of electron spin decoherence through hyperfine interaction in a quantum dot*, *Phys. Rev. B* **73**, 241303 (2006).
- [40] G. W. Morley, J. van Tol, A. Ardavan, K. Porfyraakis, J. Zhang, and G. A. D. Briggs, *Efficient dynamic nuclear polarization at high magnetic fields*, *Phys. Rev. Lett.* **98**, 220501 (2007).
- [41] S. Sangtawesin, C. A. McLellan, B. A. Myers, A. C. B. Jayich, D. D. Awschalom, and J. R. Petta, *Hyperfine-enhanced gyromagnetic ratio of a nuclear spin in diamond*, *New J. Phys.* **18**, 083016 (2016).
- [42] R.-B. Liu, W. Yao, and L. Sham, *Control of electron spin decoherence caused by electron–nuclear spin dynamics in a quantum dot*, *New J. Phys.* **9**, 226 (2007).
- [43] W. Yao, R.-B. Liu, and L. J. Sham, *Theory of electron spin decoherence by interacting nuclear spins in a quantum dot*, *Phys. Rev. B* **74**, 195301 (2006).